SE9800004

ISRN KTH/ALP/R--97/3--SE

KTH

Interacting Eigenmodes of a Plasma Diode with a Density Gradient

T. Löfgren and H. Gunell

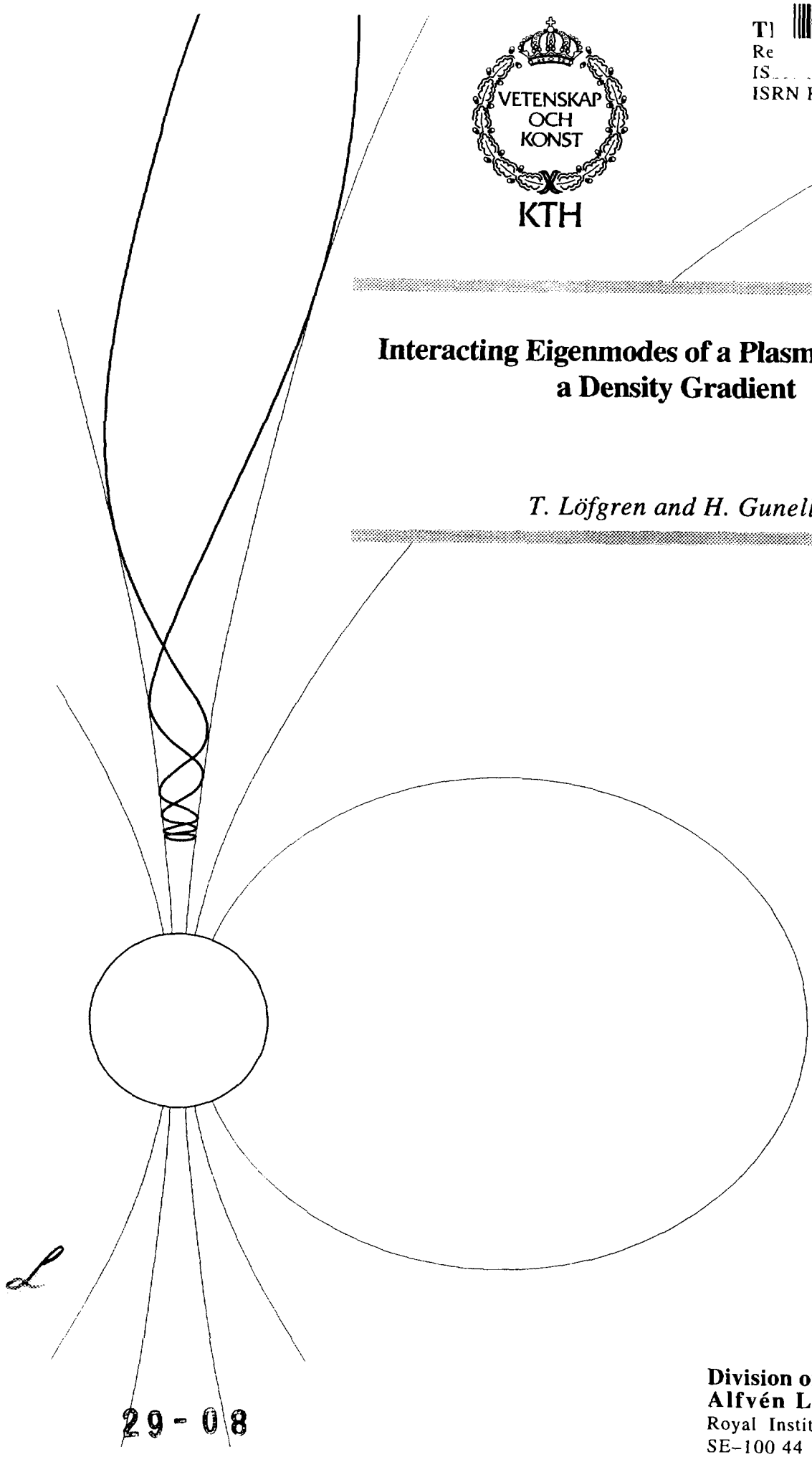

29-08

Division of Plasma Physics
Alfvén Laboratory
Royal Institute of Technology
SE-100 44 Stockholm, Sweden

TRITA-ALP-1997-03
ISSN 1103-6613

Interacting eigenmodes of a plasma diode with a density gradient

T. Löfgren and H. Gunell

Division of Plasma Physics, Alfvén Laboratory,
Royal Institute of Technology, SE-100 44 Stockholm, Sweden

The formation of narrow high frequency electric field spikes in plasma density gradients is investigated using one-dimensional particle in cell simulations. It is found that the shape of the plasma density gradient is very important for the spike formation. The spike appears also in simulations with immobile ions showing that a coupling to the ion motion, as for example in wave-wave interactions, is not necessary for the formation of HF spikes. However, the HF spike influences the ion motion, and ion waves are seen in the simulations. It has been found, in experiments and simulations, that the electron velocity distribution function deviates from the Maxwellian distribution. Dispersion relations are calculated using realistic distribution functions. The spike can be seen as a coupled system of two eigenmodes of a plasma diode fed by the beam-plasma interaction. Based on a simplified fluid description of such eigenmodes, explanations for the localization of the spike, spatially and in frequency, are given. The density amplitude is comparable with the density DC level close to the cathode. Space charge limits of waves in this region seem to determine the amplitude of the spike through the Poisson's equation.

August 1997, 25pp. incl. illus., in English

Keywords: Beam-plasma experiment, Beam-plasma interaction, Dispersion relation, Distribution functions, Eigenmodes, Electron beam, Electrostatic waves, Fluid theory, HF spike, Kinetic theory, PIC simulation, Pierce diode, Plasma diode

TRITA-ALP-1997-03
Report
ISSN 1103-6613
ISRN KTH/ALP/R--97/3--SE

Interacting eigenmodes of a plasma diode with a density gradient

T. Löfgren and H. Gunell

August 1997

Division of Plasma Physics
Alfvén Laboratory
Royal Institute of Technology
SE-100 44 Stockholm, Sweden

Interacting eigenmodes of a plasma diode with a density gradient

T. Löfgren and H. Gunell

Division of Plasma Physics, Alfvén Laboratory,
Royal Institute of Technology, SE-100 44 Stockholm, Sweden

Abstract

The formation of narrow high frequency electric field spikes in plasma density gradients is investigated using one-dimensional particle in cell simulations. It is found that the shape of the plasma density gradient is very important for the spike formation. The spike appears also in simulations with immobile ions showing that a coupling to the ion motion, as for example in wave-wave interactions, is not necessary for the formation of HF spikes. However, the HF spike influences the ion motion, and ion waves are seen in the simulations. It has been found, in experiments and simulations, that the electron velocity distribution function deviates from the Maxwellian distribution. Dispersion relations are calculated using realistic distribution functions. The spike can be seen as a coupled system of two eigenmodes of a plasma diode fed by the beam-plasma interaction. Based on a simplified fluid description of such eigenmodes, explanations for the localization of the spike, spatially and in frequency, are given. The density amplitude is comparable with the DC density level close to the cathode. Space charge limits of waves in this region seem to determine the amplitude of the spike through the Poisson's equation.

1 Introduction

Beam plasma interaction occurring in density gradients can give rise to narrow (about one wavelength) high frequency (HF) electric field spikes, as shown by experiments and particle in cell simulations [1, 2, 3]. This is important for the physics of double layers where the electrons that are accelerated in the double layer are accelerated into the plasma on the high potential side. At a double layer the ratio between beam and plasma density $\eta = n_b/n_0$ is much higher than in classical beam plasma experiments. The HF spikes have been studied in a double layer experiment [1], through particle in cell simulations, and in an experiment with a hot cathode as source of the electron beam [2, 3].

Common to these studies is that the plasma density has a gradient with increasing density in the direction of the electron beam. Density inhomogeneities influence the growth of plasma instabilities, as was shown in early experiments [4, 5].

In this paper we report further results from simulations, and propose an explanation of the spatial location and frequency of the spike based on a fluid model of eigenmodes of the system. The fluid picture is complemented by kinetic calculations of wave modes and their growth rates.

A system similar to the system studied here is the Pierce diode [6]. A classical Pierce diode is a bounded system, with externally short-circuited electrodes. A cold electron beam passes through a neutralising background of immobile ions with a constant density. A modified Pierce diode with a nontrivial external circuit was studied by Hörhager and Kuhn [7], who used a fluid model to describe nonlinear steady-state oscillations. Kinetic theory was used by Kuhn [8] to find eigenmodes of a Pierce type diode, and it was found that the eigenmodes and eigenfrequencies depended on the external circuit. Another bounded plasma system of interest is the single-emitter plasma device that has been treated by e. g. Crystal et al. [9]. A review of bounded plasma systems was given by Kuhn [10].

The fluid model that is used in this paper takes into account the inhomogeneous density and the finite temperature of the plasma. Linearised dynamic equations are solved numerically.

In section 2 the particle in cell simulations are described and the results from these are presented. The power spectrum of the electric field shows two distinct peaks at approximately 114 and 228 MHz, each corresponding to one position in the inhomogeneous part of the plasma. Dispersion relations, calculated for the appropriate velocity distribution functions observed in simulations and experiments, are presented in section 3. A new method for calculation of dispersion relations is used [11]. The fluid model is developed in section 4. The numerical calculations are described, and the frequency response and the fluid eigenmodes of the diode are given. In section 5 eigenmodes of systems with different temperatures and boundary conditions are presented. An increased temperature is seen to reduce the number of eigenmodes. The new boundary condition does not qualitatively change the response of the plasma. In section 6 the conclusions are discussed, and an explanation of the formation of the HF spikes is proposed.

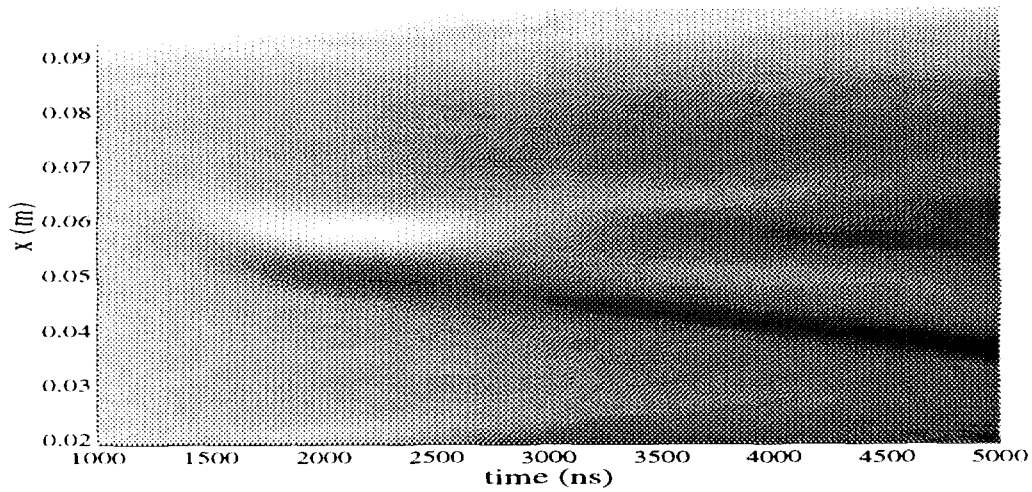

Figure 1: The momentum density of the ions as a function of time and space. Ion waves are seen to move in both directions. The phase velocity of the forward wave is 3.5 km/s and the phase velocity of the backward wave is 5 km/s.

2 PIC-simulations

The simulations were performed using the 1D electrostatic particle-in-cell code, PDP1 [12]. In the previously reported simulations [2, 3] the plasma parameters used in the simulations were chosen as close to the experimental parameters as possible. Different experimental cases with various acceleration voltages were simulated. A description of the experimental setup is given in reference [3]. In this work we concentrate on the case with 95 V acceleration voltage, and perturb the simulated system in various ways in order to find which processes are important for the formation of the HF spike.

The plasma was simulated using a 300 mm long, short circuited, plasma diode, and the background electron temperature was 6 eV. The initial density increased linearly from zero at the left hand boundary ($x = 0$) to a constant value ($1 \cdot 10^{15}$ m^{-3}) in the right hand part of the plasma ($x > 90$ mm). A half-Maxwellian distribution of electrons, with a temperature of 0.15 eV for the full Maxwellian distribution, was injected at $x = 0$ and accelerated in a cathode sheath that developed self-consistently. These electrons formed the beam. A narrow region of standing waves at high amplitude, the HF spike, developed at $x \approx 50$ mm. These simulations are further described in reference [3].

The influence of the HF spike on the motion of the ions has been investigated by simulations. These simulations were made using the same parameters as in the previously reported 95 volt case [3]. The simulated system was divided into 2 mm long bins, and the sum of the velocities of the ions was recorded at 50 nano-second intervals. The thus obtained quantity is proportional to the ion momentum density. Fig. 1 shows the ion momentum density in a grey-scale diagram for times between 1μs and 5μs. It is seen from Fig. 1 that ion waves are generated at the position of the HF spike, and that they travel in both directions. The phase velocity of the forward travelling ion wave is estimated to 3.5 km/s, and the phase velocity of the backward wave is 5 km/s. The sound speed for argon at 6 eV is 3.8 km/s. The electron

temperature in this region is slightly higher. The difference between the two propagation directions is possibly an effect of systematic ion motion towards the cathode.

It has been hard to find parameters that give clear spike patterns. There is too few observations to make it possible to predict the region in the parameter space where the spike exists. But by starting from a situation where the spike has formed the system can be perturbed in order to gain information about the conditions that are necessary for spike formation. After $t = 2\mu$s in the simulation of the 95 V case [3] an HF spike is clearly seen. A perturbation was introduced at this time ($t = 2\mu$s) by removing all electrons and replacing them with the initial ($t = 0$) thermalized phase space distribution of the electrons. After some transient oscillations the spike reappeared after approximately 100 ns, which is a few transit times through the system of electrons resonant with typical waves.

A similar perturbation experiment was performed by removing all ions at $t = 2\mu$s, and replace them with the initial ($t = 0$) phase space distribution of the ions. This perturbation caused the disappearance of the spike. Hence the spatial ion-distribution is important in spike formation. Another replacement experiment was made by replacing the ions with a background of positive charge that is constant in time and follows $n_{ion}(x)$ at $t = 2\mu$s. In this case there are no mobile ions, and we cannot have any coupling to ion waves. But the rigid background can transfer momentum to electron waves. A spike is still seen in this kind of experiment. Hence we conclude that the ion density as a function of space $n_{ion}(x)$ is important for the formation of an HF spike, and that ion motion is not necessary for spike formation. The remaining part of this paper is restricted to electron behaviour with rigid ion background. The effects of the ion-motion on these results will be briefly discussed in sec. 6.

A simulation was run with a background of positive charge instead of ions. The acceleration voltage was 95 V, and as in the simulations described in [3] an HF spike appeared at $x \approx 55$ mm. The electric field as a function of time is shown in Fig. 2 for five times t between $t = 532$ ns and $t = 534$ ns. The local character of the field spike is evident in Fig. 2(a). The quite high and constant level of the electric field at frequencies well below the plasma frequency in the homogeneous region, Fig. 2(b,c), is a result of net currents through the system. In Fig. 3 contours of the FFT-amplitude of the electric field, in a simulation with 95 V acceleration voltage, are shown. There are two local maxima of the electric field amplitude in the inhomogeneous region of the plasma. The maxima appear at $x_1 = 1.5$ cm and $x_2 = 5.5$ cm. The maximum at x_2 is identified as the HF spike. The frequencies f_1 and f_2 at $x = x_1$ and $x = x_2$ are close to, but above, the plasma frequencies at these points. The frequencies are related by $f_2 \approx 2f_1$. The distance $x_2 - x_1$ contains an integer number of wavelengths for a Langmuir wave travelling backwards from x_2 to x_1. The two frequencies are evident in the outer circuit current, see Fig. 4, which suggest that the spike is not a localized but rather a systemwide phenomenon. The power content of the current at the two frequencies corresponds to two harmonic currents with amplitudes of 6.5 Am^{-2} and 3.5 Am^{-2} respectively.

These observations leads to the following hypothesis. There are two cou-

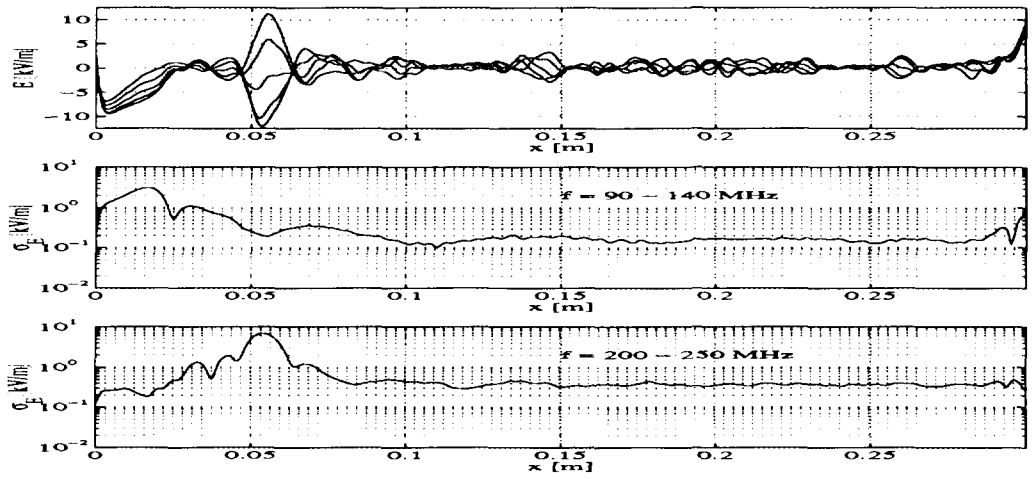

Figure 2: (a) The electric field as a function of time for five times t between $t = 532$ ns and $t = 534$ ns. The simulation was run with a background of positive charge instead of ions. (b,c) The root mean square value (RMS) of the electric field in frequency bands around the dominant frequencies (seen in Fig. 3). The shown RMS-value is the standard deviation of the electric field after it has been filtered by tenth order Butterworth bandpass filters. The original data was a 1.024 μs series with sampling frequency 2 GHz. The standard deviation in (c) increases nearly two orders of magnitude from the cathode to the spike. The standard deviations in (b,c) have high and nearly constant values in the homogeneous plasma region where these frequencies are well below the local plasma frequency 284 MHz.

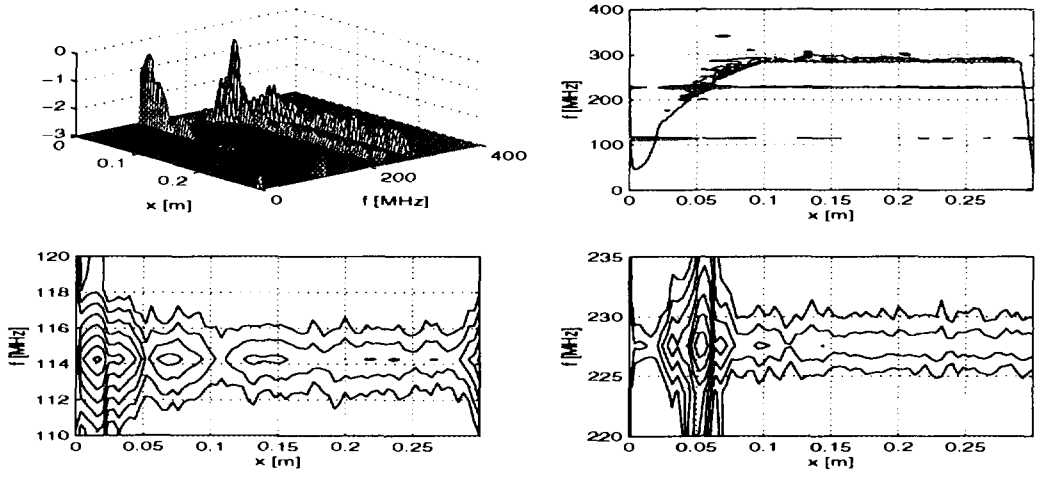

Figure 3: FFT power of the electric field calculated from 1.024 μs time series with 2 GHz sampling frequency. The shown values are normalized to the maximum power which corresponds to a harmonic field with amplitude of ~11 kV/m. (a) The 10-logarithm of the power with the minimum limited to 10^{-3} of the maximum amplitude (for readability). (b-d) are logarithmic contour graphs. Two contours per power of ten are shown. The lowest contour shown in (b,d) is 10^{-3} and the lowest contour in (c) is 10^{-4}. The two pronounced frequencies (enhanced in (c,d)) have the maximum amplitudes a fraction of a wavelength before $f = f_p$. The local plasma frequency f_p is shown as reference in (b). Note in (c,d) that there is several spatial maxima and note also that the oscillations extends with constant amplitude into the region where $f < f_p$.

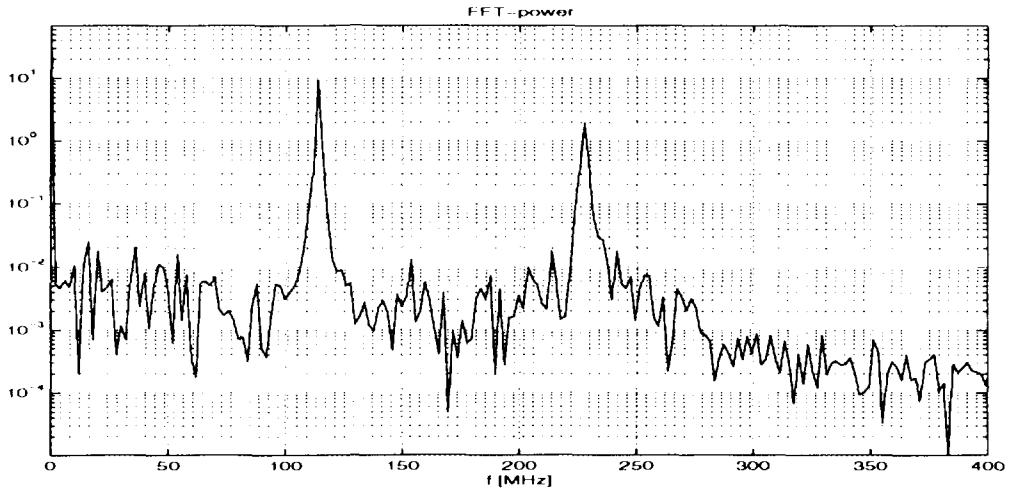

Figure 4: FFT power of the outer circuit current. The spectrum is calculated from a 500 ns time series with a 1 GHz sampling frequency. The two frequencies $f \sim 114, 228$ MHz coincide with the localized spikes in Fig. 3.

pled eigenmodes of the diode. The eigenmode with maximum amplitude at x_1 pre-modulates the beam, that is not yet fully accelerated. At x_2, the location of the maximum amplitude of the second eigenmode with frequency $2f_1$, i.e., twice the modulation frequency, plasma oscillations grow to high amplitude. Since waves at the frequency f_2 cannot propagate into the higher density plasma at $x > x_2$ the waves are reflected, and the Langmuir wave travelling back towards the cathode feeds the pre-modulating oscillation at x_1. The growth and reflection of the forward wave, together with the damping of the backward wave accounts for the narrowness of the spike.

The location of the spike spatially and in frequency are treated by linearized equations in the following sections. The electron density is recorded during 100 ns and the results are shown in Fig. 5. The standard deviation σ_n is small ($\sigma_n \ll n$) in most part of the diode and the linearizations are justified. But close to the cathode not only the linear picture breaks down. The amplitude of the oscillations is space charge limited, i.e., the density amplitude is limited by the DC density level. If the spike is a global phenomenon the amplitude limits close to the cathode will determine the amplitudes in the whole diode.

3 Dispersion relations

Dispersion relations are needed to know which wave modes that can be present in the plasma. Kinetic calculations of these dispersion relations will give more accurate growth rates for the unstable wave modes than those obtained from fluid theory. The dispersion relations for Langmuir and beam waves in plasmas where the electrons follow the Maxwellian velocity distribution are well known. In the present case the distribution function deviates significantly from the Maxwellian distribution. The beam electrons are accelerated in the cathode sheath, and even though they are spread in velocity space, when they pass the HF spike, they still have higher energy than most

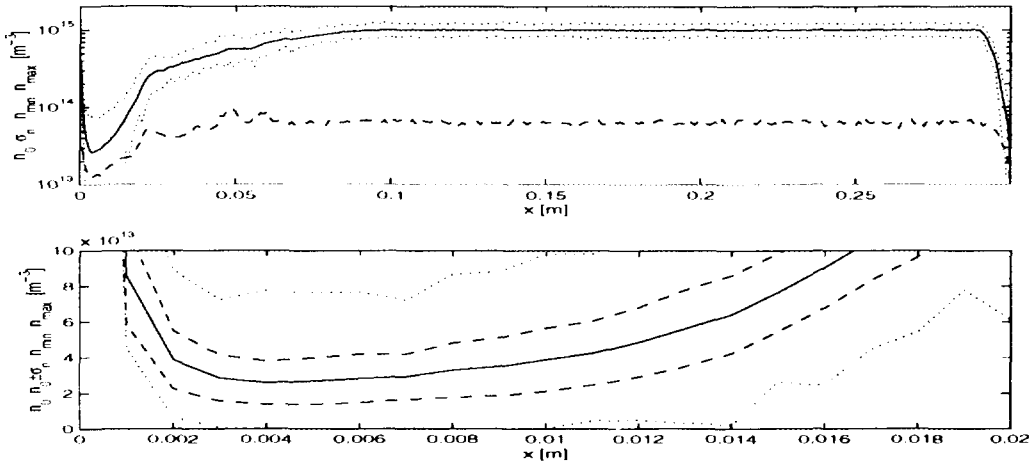

Figure 5: The electron density recorded during 100 ns. The time-average n_0 is shown as solid lines and the extreme values (min/max) are given as dotted lines. In (a) the dashed line is the standard deviation σ_n and in (b) they are $n_0 \pm \sigma_n$. Note that the scale is logarithmic in (a) but linear in (b). The (b) figure is a magnification of the region with space charge limited oscillations close to the cathode.

bulk electrons. The plasma is hence receiving electrons at high velocity, yielding tails in the distribution function that are thicker than the Maxwellian tails. At the anode in the simulations, and at the floating plate in the experiment [3] electrons with energy over a certain limit are lost, and electrons with lower energy are reflected. This leads to a cutoff in the distribution function. There is a similar reflection at the cathode, but since the cathode is the most negative point in the system almost all electrons reaching it are reflected. A measurement of the electron distribution function is presented in Fig. 6. The measurement was made with a small gridded analyser in the middle of the experimental device, described in reference [3], 30 cm from the cathode. The apparent decrease in the distribution function at low energies is due to radial loss to the inner walls of the analyser. The electron gyro radius and the dimensions of the analyser are comparable, and some electrons that reach the first grid with low energy in the beam-direction are able to reach the walls before they reach the collector. The analyser shadows the a region on its magnetic flux tube between itself and the floating plate (see the description of the experiment in reference [3]). Hence the electrons that occupy this region must have drifted into that flux tube across the magnetic field lines. Hence the measured distribution function for electrons with negative v is smaller than the distribution function for electrons with positive v. The cutoff in the distribution function is seen as a decrease in the distribution function around 80 eV energy for the electrons travelling towards lower x. The thick tails appear in both directions, but it is most clearly seen for electrons with positive v.

The present distribution functions are approximated by rational functions and dispersion relations are calculated using a recently developed method [11]. The velocity distribution function f_e is described by an expansion that has a finite number of simple poles, which gives efficient numerical calcula-

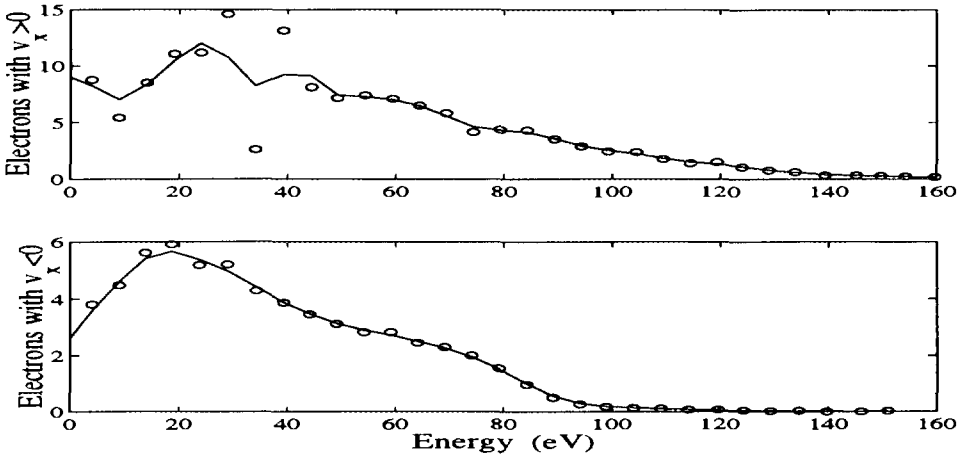

Figure 6: A measurement of the electron distribution function for electrons moving towards higher x (upper panel), and lower x (lower panel). The high velocity tails are thicker than the Maxwellian tails, and there is a cutoff at 80 eV for electrons with $v < 0$.

tions and control of all converging moments

$$f_e(\xi) = NM_w(\xi)T(\xi), \quad \xi \equiv (v - v_d)/v_t, \tag{1}$$

where v_d is the drift velocity, v_t is the thermal velocity and N is a normalization factor. $M_w(\xi)$ is a warm expansion of the Maxwellian distribution and $T(\xi)$ is a mask that is introduced to suppress the distribution above the cut energy. These terms are given by

$$\begin{aligned} M_w(\xi) &= \left[1 + \tfrac{\xi^2}{2} + \cdots + \tfrac{1}{m!}\left(\tfrac{\xi^2}{2}\right)^m\right]^{-1}, \\ T(\xi) &= \left[1 + \left(\tfrac{\xi}{\xi_0}\right)^{2n}\right]^{-1}. \end{aligned} \tag{2}$$

The low velocity region of f_e is Maxwell-like and the high velocity tail follows an inverse power law.

The density ratio and the beam velocity change considerably along the gradient. The linear (Vlasov-Poisson) dispersion roots for a homogeneous plasma with parameters at the spike position are given in Fig. 7. A superposition of a background distribution and a beam distribution, each expanded as in Eqs. 1,2, is used. There is three important roots, the Langmuir roots (LW1,LW2) in the two propagation directions and the,slow space charge wave (SSCW). The solid lines give the result for distributions with thick tails and the dashed lines are the result for a distribution with a cut at 40 eV in the stationary distribution. This cut is the result of non-reflection of high energy electrons in the anode sheath. The anode potential drop 40 eV coincide with the potential drop in the PIC-simulations and with the potential profile in the fluid description in the sections 4 and 5, see Fig. 9. The real part of ω is only slightly modified by the cut. The cut greatly reduces the Landau damping of the Langmuir roots and slightly increases the growth rate of the slow space charge wave. The SSCW and LW2 above the plasma frequency have no mirror wave with opposite phase velocity. If the spike is a composition

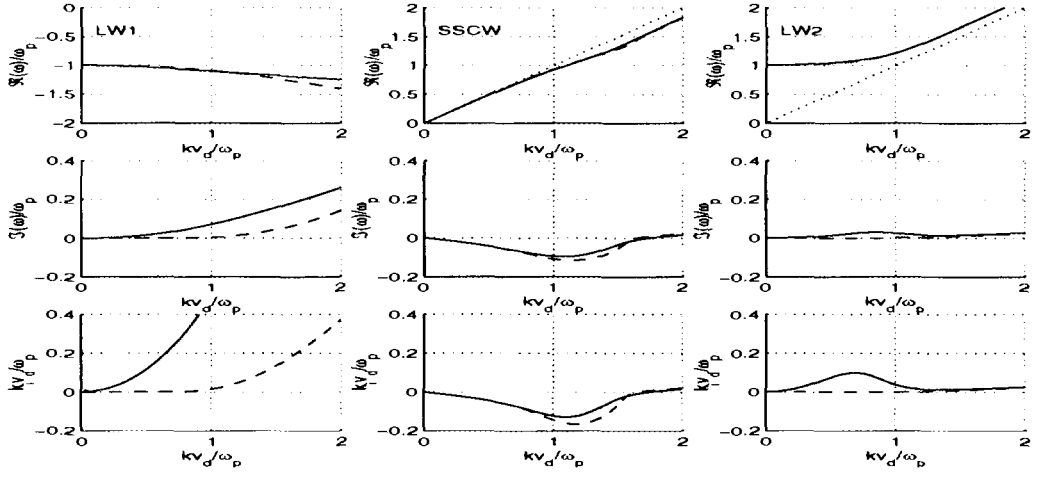

Figure 7: Dispersion roots for parameters close to the spike. The left panels give the backward Langmuir wave. The mid panels show the slow space charge wave which is the wave mode with growing solutions. The right panels give the Langmuir wave in the beam direction and its connection to the fast space charge wave. The electron number density n_0 is $0.6 \cdot 10^{15}$ m^{-3} ($\omega_p = 1.4$ GHz) and the beam drift velocity v_d is $5.8 \cdot 10^6$ m/s (95 eV). Other parameters for the (background, beam) components are the density $n = (0.99, 0.01)n_0$ and the thermal velocity $v_t = (0.2, 0.03)v_d$ ($\sim (6, 0.15)$ eV). The solid lines give the result for distributions with thick tails and the dashed lines are the result for a distribution with a cut at 40 eV in the stationary distribution. The used expansion parameters are (detailed description in [11]): $m = (2, 4)$, $n = (0/4, 0)$ and $\xi_0 = (0.65, 0)$. The real part is displayed in the upper panels and the imaginary part is shown in the mid panels (growing modes have negative imaginary part). The lower panels give approximative spatial growth rates $k_i = \Im(\omega)/|\frac{\partial \Re(\omega)}{\partial k}|$. By the use of absolute value of the group velocity the growing solutions have negative k_i.

of forward waves and reflected backward waves, standing waves will appear close to the reflection point. Closer to the cathode the wavelength mismatch and the damping of the reflected wave will cause the electric field to be more traveling wave like as reported in [3]. The growth rates are reduced in inhomogeneous systems [5] but the homogeneous estimates can serve as an upper limit. Closer to the cathode the relative beam density is larger than at the spike. Not even at those parameters the spatial growth rate k_i get larger than $\sim 0.2\omega_p/v_d$. With the parameters at the spike this gives $k_i \sim 47$ m^{-1}. The region with low v_d does not give higher growth. Most of the beam acceleration takes place in the first centimetre of the cathode sheath and this region is practically free from stationary background electrons. A given frequency ω can have the maximum growth in one single point at the density gradient. In other positions of the system, waves of this frequency can have low growth or they can be damped. By assuming homogeneous plasma in the calculation of k_i and further assuming the maximum k_i to be global for a given frequency, overestimated amplitudes are obtained. A factor of 10 in the growth of the electric field from the cathode to the spike can be explained by this optimistic estimate. The electric field amplitude in Fig. 2 (c) increases nearly two orders of magnitude from the cathode to the spike. A linear beam-plasma instability can not explain the high amplitude at the spike.

4 Fluid eigenmodes in a diode

The nature of the HF spike as an interference of a forward and a reflected backward travelling wave was described in sec. 2. From the PIC-simulation it is clear that the spike frequency and a subharmonic are present in the whole system. This suggest that the phenomenon is not localized but systemwide. As was seen in Fig. 3, frequencies below the local plasma frequency are present in the homogeneous plasma region. Some questions are then: What eigenmodes does the plasma diode support and which parameters influence the resonant frequencies? How can the waves survive in the evanescent regions?

Fully kinetic solutions of the (non-linear) beam-plasma interaction in density gradients are only reachable with the use of PIC-simulations. The PIC-simulations are too noisy and time consuming to study frequency response of the diode, and the results are hard to interpret. As it will turn out, an understanding of the frequency response can be obtained, and some of the observations can be explained, within the framework of a fluid-model. Linearized dynamic equations capturing the inhomogeneities, the finite extension as well as the electrostatic fields will be used. The solution is obtained in a two step procedure. First a static solution is found, and secondly those results are used as inputs in the dynamic equations.

The static electric field (index 0 on static variables) $E_0 = -\frac{\partial \phi_0}{\partial x}$ is determined from Boltzmann-Poisson equations and boundary conditions. The left/right potential ($\phi|_{x=0,L}$), the electron density at plasma potential (n_p, ϕ_p) and the ion density profile $n_{ion}(x)$ are taken from the PIC-simulation. The ions have infinite mass and the density profile does not follow the Boltzmann

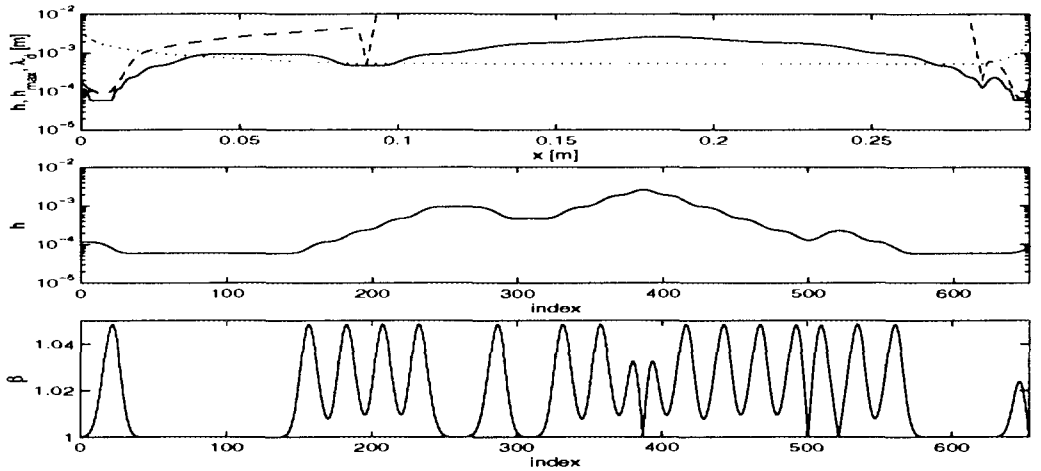

Figure 8: (a) The chosen step length h (solid), the maximum step length $h_{\max}$ (dashed) and the electron Debye length λ_D (dotted) in the static solution displayed in Fig. 9. (b) The step length as function of index to enhance the smoothness of the discretization. The incremental factor β in (c) $h_i = \beta^{\pm 1} h_{i-1}$ has a wavy but low value from the spatially localized refinements and filtering.

law. The profile is chosen in order to model the experiment, as shown in Fig. 9. In the experimental plasma there are different ionization rates in different regions, radial and axial losses.

$$\left.\begin{array}{c} n_0 = n_p \exp \frac{e(\phi_0 - \phi_p)}{k_B T_e} \\ \frac{\partial^2 \phi_0}{\partial x^2} = \frac{e(n_0 - n_{ion})}{\epsilon_0}, \quad 0 < x < L \\ \phi|_{x=0,L}, \ (n_p, \phi_p) \end{array}\right\} \tag{3}$$

A (nonlinear) Finite Difference representation of these equations is

$$\left.\begin{array}{l} 0 = x_0 <, \ldots, < x_n = L, \ h_i = x_i - x_{i-1}, \ \phi_i = \phi_0(x_i) \\ \left\{\begin{array}{l} \mathcal{D}_2 \phi_i = 2 \frac{h_{i+1}\phi_{i-1} - (h_{i+1}+h_i)\phi_i + h_i \phi_{i+1}}{h_i h_{i+1}^2 + h_i^2 h_{i+1}} \\ \delta_i = \mathcal{D}_2 \phi_i + \frac{e}{\epsilon_0}(n_{ion} - n_p \exp \frac{e(\phi_i - \phi_p)}{k_B T_e}), \quad j = 1 \ldots (n-1) \\ \delta_0 = \phi_0 - \phi(x=0), \ \delta_n = \phi_n - \phi(x=L) \end{array}\right. \\ \delta_i = 0, \quad \forall i \in [0 \ldots n] \end{array}\right\} \tag{4}$$

where $\mathcal{D}_2$ is the discrete Laplace operator and δ_i is the local error in Poissons equation. To handle long system and still resolve local scale lengths, a nonuniform grid size $\{h_i\}$ is chosen. With $\mathcal{D}_2 \phi_i = \phi''|_{x_i} + \frac{1}{3}\phi'''|_{x_i}(\frac{h_i h_{i+1}^3 - h_i^3 h_{i+1}}{h_i h_{i+1}^2 + h_i^2 h_{i+1}}) + \mathcal{O}(h^2)$, it is evident that a nonuniform grid size reduces the order of the error term in $\mathcal{D}_2$ from quadratic to linear. If h_i varies slowly the error term is practically quadratic. The step length is thus calculated iteratively for finer an finer discretization such that $h_i < h_{\max} \equiv 0.05\sqrt{\frac{k_B T_e}{e\phi''}}$ and such that successive step lengths differ with at most a factor of 1.05, see β in Fig. 8.

Eq. 4 is a nonlinear equation system in ϕ_i and the solution is to be found by iterative methods. If the quantities in iteration l will be marked with an upper index, a fast converging (Newton-Raphson) iteration step is found by solving the linear system $\sum_j \frac{\partial \delta_i^l}{\partial \phi_j}(\phi_j^{l+1} - \phi_j^l) + \delta_i^l = 0$. This solution method has been used in the presented results in Fig. 9 since it is fast converging and the

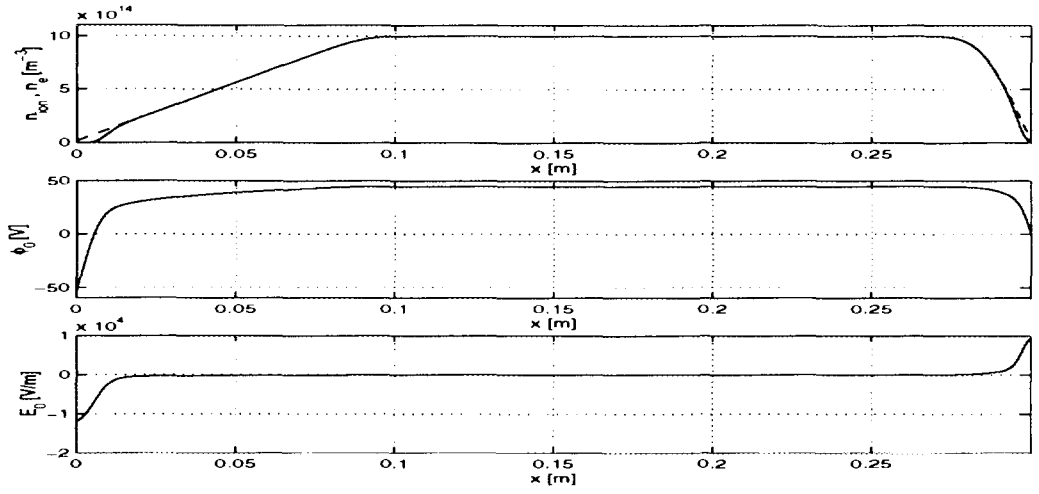

Figure 9: (a) Ion density (n_{ion}) in input (dashed). (a-c) The electron density (n_0) (a solid), the static potential (ϕ_0) and the static electric field E_0 obtained from numerical solution of Eq. 3. The used input parameters are $n_p = 10^{15}$ m^{-3}, $\phi_0(x = 0) = -55$ V, $\phi_0(x = L) = 0$, $\phi_p = 40$ V and the electron temperature 10 eV.

functional matrix $\frac{\partial \delta_i^l}{\partial \phi_j}$ is analytically known, simple and sparse. Alternatively the solution can be obtained by minimization algorithms, e.g., the steepest descent method, applied to the problem $\min_{\{\phi_i\}} \sum \delta_i^2$.

A small amplitude ($|n_1| \ll n_0$) time varying component is added to the system. The static variables will have index 0 and the (not necessarily small) time dependent component will have index 1. The momentum balance, continuity and Poisson equations read

$$\left.\begin{array}{c} m(n_0 \frac{\partial v_1}{\partial t} + v_0 \frac{\partial n_1}{\partial t}) = -e(n_0 E_1 + n_1 E_0) - \gamma k_B T_e \frac{\partial n_1}{\partial x} \\ \frac{\partial n_1}{\partial t} + \frac{\partial}{\partial x}(n_0 v_1 + n_1 v_0) = 0 \\ \frac{\partial E_1}{\partial x} = -\frac{e n_1}{\epsilon_0} \end{array}\right\}. \qquad (5)$$

The neglected convective derivative $v\frac{\partial}{\partial x}$ is small in most of the examples below. In Fig. 10 some velocities from the PIC-simulation are shown. Except from the leftmost part of the diode the velocities v_0, v_1 are of the order 10^5 m/s or lower. The wavelengths are of the order of centimetres which gives an estimate $v\frac{\partial}{\partial x} \sim 10^7$ s^{-1}. The time derivative can be estimated by the angular frequency at the spike $\frac{\partial}{\partial t} \sim \omega \sim 10^9$ s^{-1}. As long as higher frequencies are concerned it is justified to neglect the convective derivative. The temperature of the electrons has increased to about 8 eV in the homogeneous region ($v_t \sim 1.2 \cdot 10^6$ m/s). The fluid description fails in describing the plasma in the first centimetre, where the beam is dominant, the drift velocity is important and the linearization fails. These deviations from the idealized fluid description will be discussed in Sec. 6. The static electric field is large in the sheath and presheath regions ($|E_0| \gg |E_1|$ in the PIC-simulation) and the term $n_1 E_0$ is consequently kept. The drift v_0 is not large. The term $v_0 \frac{\partial n_1}{\partial t}$ can be kept or neglected without any significant modifications. It enters as an extra contribution in the total current below. The linear approximation is thus limited to the requirements that $v_1 \frac{\partial n_1}{\partial t}$, $n_1 E_1$, and the convective derivative are neglectable.

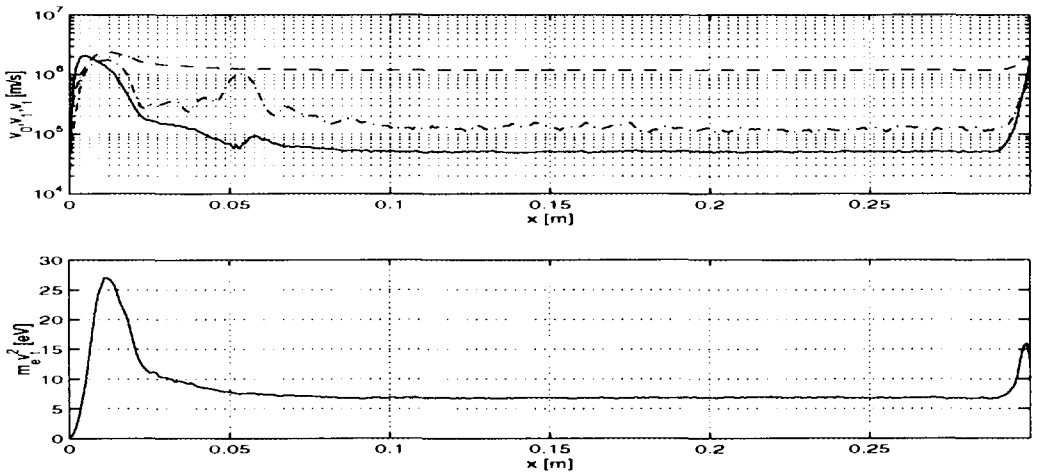

Figure 10: (a) Different moments of the distribution function in the PIC simulation described in Sec. 2. The moments are calculated using 0.5 mm bins and taking time averages (marked with a bar) over 100 ns. The DC drift $v_0 = \overline{< v >}$ is shown as a solid line, the thermal velocity $v_t = \sqrt{\overline{< v^2 > - < v >^2}}$ is displayed as a dashed line. The dash-dotted line is a root mean square measure of the time dependent velocity $v_1 = \sqrt{\overline{(< v > - v_0)^2}}$. In (b) the temperature is shown with linear scale.

With harmonic time dependence, $\frac{\partial}{\partial t} = i\omega$ and some algebraic steps, Eq. 5 reduces to

$$\mathcal{D}E_1 \equiv \frac{\gamma k_B T_e}{m}\frac{\partial^2 E_1}{\partial x^2} + \frac{eE_0(x)}{m}\frac{\partial E_1}{\partial x} + (\omega^2 - \omega_p^2(x))E_1 = -\frac{i\omega}{\epsilon_0} j_T \qquad (6)$$

where j_T is the total, spatially invariant, current density $-e(n_0 v_1 + n_1 v_0) + i\omega\epsilon_0 E_1$ and $\omega_p^2(x) = e^2 n_0(x)/(m_e\epsilon_0)$. The boundary conditions are chosen as

$$\left.\begin{aligned} E_1|_{x=0} &= -\alpha_0 \tfrac{i}{\omega\epsilon_0} j_T \\ E_1|_{x=L} &= -\alpha_L \tfrac{i}{\omega\epsilon_0} j_T \end{aligned}\right\} \qquad (7)$$

where $\alpha_{0,L}$ are dimensionless constants. Before dealing with the numerical solution some general properties of Eq. 6 and the boundary conditions in Eq. 7 will be discussed.

- The boundary conditions with $\alpha_0 = \alpha_L = 1$ are equivalent with the requirement of no oscillating particle currents at the diode boundaries. With $\alpha_{0,L} = 0$ there are no displacement currents at the boundaries. With general complex $\alpha_{0,L}$ inside the unit circle there is both particle and displacement currents with different phase at the boundaries. If there is a stationary plasma $v_0 = 0$ and the plates are non-emitting it is impossible to have any particles leaving the plates. The particle current must therefore be zero since any nonzero amplitude requires emission during half of the period ($\alpha_{0,L} = 1$). As seen in Fig. 10 $v_0 \neq 0$ and the boundary condition is questionable. As long as $\alpha_{0,L} \in \Re$ there are only purely standing wave solutions to Eq. 5. Imaginary $\alpha_{0,L}$ give a mixture of standing waves and travelling waves. Solutions with $\alpha_{0,L} = 0$ will be calculated and discussed in Sec. 5 to test if the description with $\alpha_{0,L} = 1$ is robust to changes in the boundary condition.

- For a frequency below the maximal (and above the minimal) plasma frequency there is two solution types. In regions where $\omega > \omega_p(x)$ there are free wave solutions and in regions where $\omega < \omega_p(x)$ there are evanescent wave solutions. The transit is not exactly at $\omega = \omega_p(x)$ if $E_0 \neq 0$.

- The evanescent wave solution does not approach zero if there is a net current j_t through the system. In homogeneous regions $\frac{dn_0}{dx} = 0$ with $\omega < \omega_p$, the solution E_1 aproaches the particular solution $-i\frac{\omega}{(\omega^2-\omega_p^2)\epsilon_0}j_T$ The two currents in the PIC-simulations are 6.5 Am^{-2} and 3.5 Am^{-2} at $\omega = 0.4\omega_p$ and $\omega = 0.8\omega_p$ respectively. The particular solutions to the fluid model with these parameters are $|E_1| = 0.30$ kV/m and $|E_1| = 0.49$ kV/m, which is in good agreement with the amplitudes $\sqrt{2}\sigma_E$ in Fig. 2.

- The solution E_1 has three degrees of freedom or independent parameters. Two degrees of freedom comes from the second order in the differential equation. The total current can also be varied independently of general boundary conditions. By the choice of the specific boundary conditions above the remaining number of degrees of freedom is reduced to one (if α given). The solutions depend only on the one-dimensional parameter space spanned by j_T.

- The equation and the boundary conditions are homogeneous of degree one in j_T and E_1, i.e., the impedance of a diode with cross section area A, $Z(\omega) = \left[\int_0^L E_1 dx\right]/(Aj_T)$, is independent of the current j_T. All solutions E_1 can be obtained by linear rescaling of the solution for a specific j_T. Since the boundary potentials are locked by the short circuit of the outer circuit, the system can sustain current driven oscillations only close to resonances $Z(\omega) = 0$. This outer circuit condition determines the eigenmode frequencies in the diode.

- As mentioned above, the linear model break down close to the cathode. In fact, the amplitudes will be space charge limited in this region, see Fig. 5. By extrapolating the linear results to the limiting amplitudes rough estimates of the maximum field amplitudes can be obtained.

The remaining part of this section describes the used numerical method and some numerical solutions of Eqs. 6, 7. The derivation aims at finding eigenmode frequencies of the diode and to explain the localization of the spike. Since regions with wave type solutions (and/or high E_0) requires a much finer discretization than the evanescent regions, an adaptive mesh finite element (FEM) solver will be used to solve Eq. 6. The FEM method easily handle a non-equidistant mesh and it also capture the gradients in the coefficients in a natural way. To determine the stepsize, the local properties of the solution is studied. If E_{hom} solves the differential equation for homogeneous plasma with the fixed coefficients evaluated at x_0, i.e., $E_0(x) = E_0(x_0)$, $\omega_p(x) = \omega_p(x_0)\ \forall x$, then $\mathcal{D}E_{\mathrm{hom}} - \mathcal{D}E_1 = \mathcal{O}(x - x_0)$. Up to second derivatives the two solutions E_{hom} and E_1 are identical. [These results can be checked by inserting $E_1 = E_{\mathrm{hom}}|_{x_0} + E'_{\mathrm{hom}}|_{x_0}(x - x_0) + \frac{1}{2}E''_{\mathrm{hom}}|_{x_0}(x -$

$x_0)^2 + \mathcal{O}((x-x_0)^3)$ and the Taylor expansions of the coefficients in the differential equation.] The curvature of the solution (and consequently the grid size) is thus determined by the locally evaluated characteristic roots q_i to the original problem

$$\frac{\gamma k_B T_e}{m} q^2 + \frac{eE_0(x)}{m} q + (\omega^2 - \omega_p^2(x)) = 0. \tag{8}$$

In the wave solution region $1/|q_i|$ has to be resolved, but in the evanescent regions it is a waste of numerical efforts to resolve $1/|q|$. To resolve the deviation from the constant particular solution, variable substitutions have to be made to avoid the cancellation problems in this region. The errors in $Z(\omega)$ will also, only be marginally reduced by resolving $1/|q|$ in there. The chosen discretization is therefore

$$\left.\begin{array}{c} 0 = x_0 <, \ldots, < x_n = L, \;\; h_i = x_i - x_{i-1} \\ h_i \leq 0.05/\max_{\{j\}} |\Im(q_j(x_i))| \\ h_i^2 |E_1''| \leq 0.02 |E_{MAX}| \end{array}\right\}. \tag{9}$$

The first criterion guaranties that the all individual wavelengths are resolved and the second criterion gives a uniform distribution of the interpolation error $||E_1^{\mathrm{FEM}} - E_1||_{L^2}$ where E_1^{FEM} is the numerical interpolating solution described below, i.e., the numerical efforts are concentrated in regions with high amplitude and highly curved solution including the boundaries of the regions with evanescent solutions. Note that the discretization in the dynamic solution differs from the discretization used in the static solution despite the same notation h_i and x_i. In the second criterion, the quantity E_{MAX} is the maximum magnitude of the electric field estimated by the FEM solution and the second derivative is estimated by a smoothed version of $|\mathcal{D}_2 E_1^{\mathrm{FEM}}|$ ($\mathcal{D}_2$ is defined in Eq. 4). The used grid sizes for some frequencies are shown in Fig. 11

The finite element method transfers the ordinary differential equation (Eq. 6) with boundary conditions (Eq. 7) to a linear equation system. The linear system is found from the variational formulation corresponding to the differential equation by seeking approximative solutions in finite dimensional subspaces to the full solution space $V(E_\Gamma)$ spanned by functions fulfilling the boundary conditions. The weak (or variational) formulation corresponding to Eq. 6 is obtained by multiplying Eq. 6 with an arbitrary function η in a test space W and integrating over the the interval I

$$\left.\begin{array}{ll} \text{Find} & E_1(x) \in V(E_\Gamma) \mid \langle E_1, \eta \rangle = -\frac{i\omega}{\epsilon_0} j_T(1,\eta) \;\; \forall \eta \in W = H_0^1(I) \\ \text{where} & V(E_\Gamma) \equiv \{\nu | \nu \in H^1(I),\, \nu(0) = E_1(0),\, \nu(L) = E_1(L)\}, \\ & \langle \nu, \eta \rangle \equiv \int_0^L \left[-\frac{\gamma k_B T_e}{m} \frac{d\nu}{dx}\frac{d\eta}{dx} + \frac{eE_0(x)}{m}\frac{d\nu}{dx}\eta + (\omega^2 - \omega_p^2(x))\nu\eta \right] dx, \\ & (\nu, \eta) \equiv \int_0^L \nu\eta dx, \\ \text{and} & I \equiv \{x \mid 0 < x < L\} \end{array}\right\}. \tag{10}$$

Define finite dimensional subspaces of the solution space $V_h(E_\Gamma) \subset V(E_\Gamma)$ and the test space $W_h \subset W$. The electric field is sought in a slightly larger space $V_h \in H^1(I)$ and the solution is explicitly restricted to the solution space $V_h(E_\Gamma) \subset V_h$. The spaces are spanned by the basis functions $\nu_k \in V_h$ and $\eta_i \in W_h$. By insertion of the FEM-solution $E_1^{\mathrm{FEM}} = \sum_{k=0}^n a_k \nu_k$ into Eq. 10,

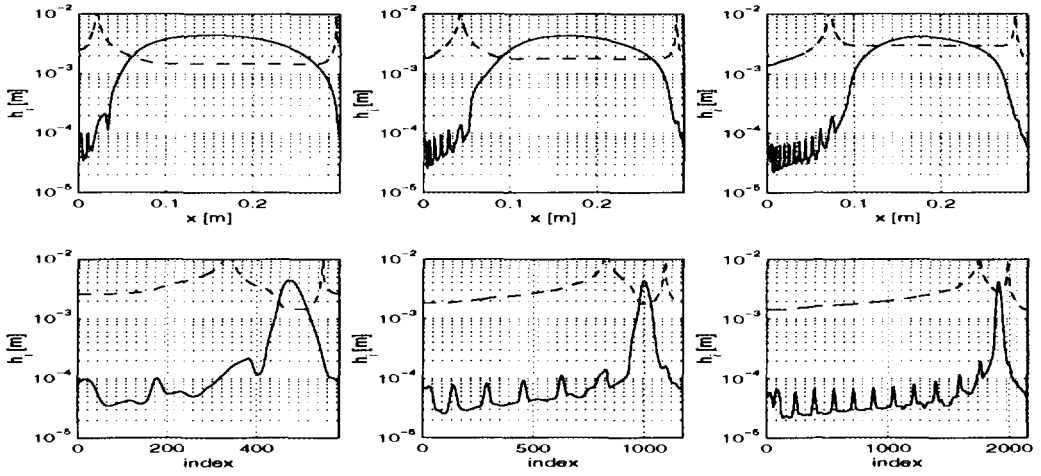

Figure 11: The step length h_i (solid) and the characteristic length $1/\max_{\{j\}}|q_j(x_i)|$ (dashed). The frequencies are $\omega = (0.5,\ 0.7,\ 0.9)\omega_{p,\max}$ in the (left, mid and right) panels, where $n_{0,\max} = 10^{15}$ m^{-3} ($f_p = 284$ MHz). The electron temperature is 10 eV and the ion profile is as shown in Fig. 9. In the upper panels h_i is given as a function of position and the lower as function of index. The fine discretization extends several decay lengths into the region with evanescent wave solutions. If the temperature is lower and/or the system is longer, the number of grid points is larger.

the variational form turns into a linear equation system in the expansion coefficients a_k

$$\left.\begin{array}{rcl} \sum_{k=0}^{n} M_{ik}a_k &=& b_i,\quad i=1,\ldots,n-1 \\ M_{ik} &=& \langle \nu_k, \eta_i \rangle \\ b_i &=& -\frac{i\omega}{\epsilon_0} j_T \int_0^L \eta_i dx \\ \sum_{k=0}^{n} a_k \nu_k|_{x=0} &=& E_1(0) \\ \sum_{k=0}^{n} a_k \nu_k|_{x=L} &=& E_1(L) \end{array}\right\}. \qquad (11)$$

The stiffness matrix M_{ik} and the load vector b_k are calculated, using piecewise linear basis functions (ν_i, η_i) with local support on $\{x \mid x_{i-1} < x < x_{i+1}, x \in I\}$, and piecewise linear coefficients $\left(\frac{\gamma k_B T_e}{m}, \frac{eE_0(x)}{m}, (\omega^2 - \omega_p^2(x))\right)$ obtained as interpolants in the static solution. The basis functions are unity at x_i, $(\eta_i(x_i) = 1)$ and zero at the interval boundaries. Note that $(\eta_0, \eta_n) \notin W_h$.

The solution is displayed in Fig. 12, for the profiles in Fig. 9 and some different frequencies. A harmonic factor $\exp(i(\omega t + \frac{\pi}{2}))$ can be multiplied with the shown solution, where the reference phase is on j_T. Higher frequencies give shorter wavelength and larger regions with wave-type solutions. The number of wavelengths in the cavity between the cathode and the reflection point thus increases fast with increasing frequency. The amplitudes are given for $j_T = 1$ Am^{-2} but the results can be linearly rescaled. The shown amplitudes have not been checked for space charge limits. They are straight forward solutions of Eq. 5. In some regions the condition $(|n_1| < n_0)$ may fail.

In Fig. 13 the position of the maximum field amplitude in the diode is given. When the frequency increases each local maximum (see Fig. 12) moves towards the cathode because of the reduced wavelength. The reflection point

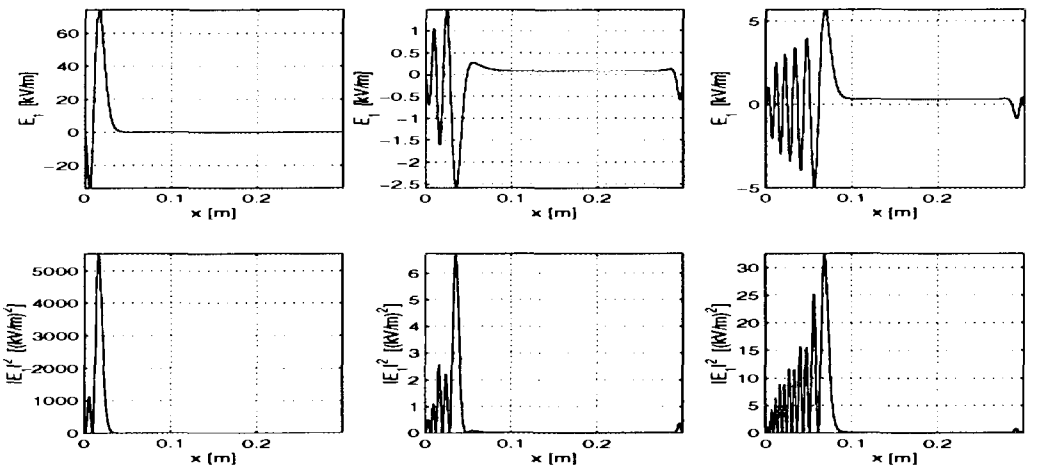

Figure 12: The electric field E_1 upper panels, and $|E_1|^2$ in the lower panels. The frequencies are $\omega = (0.5,\ 0.7,\ 0.9)\omega_{p,\max}$ in the (left, mid and right) panels, where $n_{0,\max} = 10^{15}\mathrm{m}^{-3}$ ($f_p = 284$ MHz). The total current density $j_T = 1\mathrm{Am}^{-2}$ and the electron temperature is 10 eV

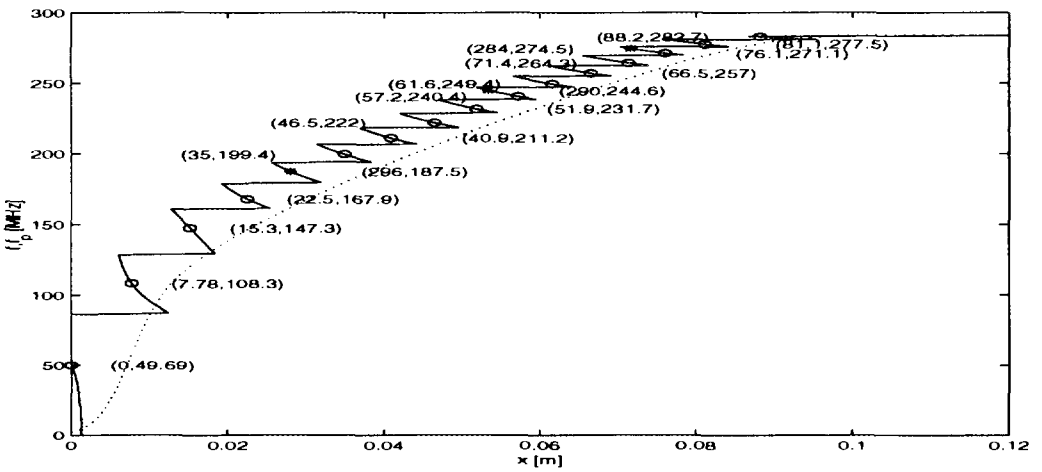

Figure 13: The sawtooth shaped line gives the position of the maximum field amplitude in the left part $x < 0.12$ m of the diode. For some frequencies this is not the global maximum. The horizontal lines represent a jump in position where two local maxima, one in each end point of the line, are equal in amplitude. Resonant frequencies with maximum in the shown region are marked with circles and resonant frequencies with global maximum in the anode sheath are marked with stars. The position of the global maximum (x [mm],f [MHz]) are given in the parenthesis. The local plasma frequency is shown as reference by the dotted line. The electron temperature is 10 eV. The static density profile and the static electric field is as shown in Fig. 9.

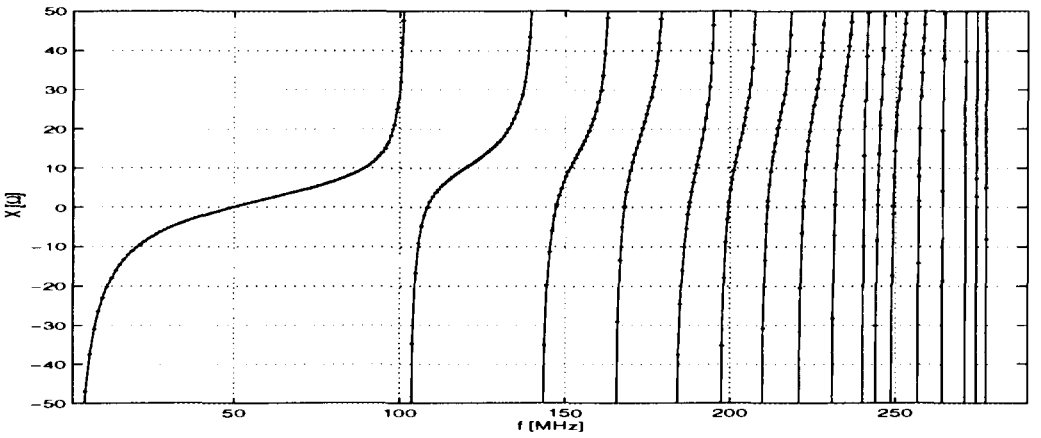

Figure 14: The reactance $X(\omega) = \Im Z(\omega)$ with diode area $A = 1$ m^2 and the electron temperature 10 eV. The static density profile and electric field is as shown in Fig. 9. The small dots are the calculated points.

moves up along the gradient. Gradually a new turn in E_1 develops between the old maximum and the reflection point. When this new turn get higher in amplitude than the previous one there is a discontinuity in the position of the spike.

The time dependent potential drop in the diode, $\phi_1|_{x=0} - \phi_1|_{x=L} = \int_0^L E_1 dx$, obtained from the solution is generally not zero. Note that the numerical integration is simple. Trapezoidal quadrature will integrate the FEM-solution exactly. The only remaining error is the interpolation error in the solution. The reactance $X(\omega) = \Im Z(\omega)$ in Fig. 14 is given for diode area $A = 1$ m^2. The discontinuities of the reactance are due to a match between the cavity and the frequency of the forced current. They represent resonances for a diode with a current source in the outer circuit and freely oscillating boundary potentials. The growing solutions are asymmetric, since each half wavelength have higher amplitude than the previous one. With unlimited amplitude in the electric field there must also be unlimited fluctuations in the boundary potentials. For a single Fourier amplitude of the current this singularity is acceptable. If the singularities remain in the time domain of the electric field, for reasonable current with nonzero bandwidth, it would imply a break down of the linear approach. In our system the boundary potentials are locked and none of these solutions are interesting.

The requirement of zero potential drop limits the system to some resonant ω with $Z(\omega) = 0$. The number of zero crossings between 0 and ω is determined by the number of half wavelengths in the solution for this ω (Figs. 12,14). To better resolve the zero crossings the inverse quantity, the admittance $|Y| = 1/|Z|$, is displayed in Fig. 15. As expected the resonances in Fig. 15 get closer for higher frequencies. The current density in the PIC-simulation (see Fig. 4) was about 3.5 Am^{-2}. The amplitude at the resonances in Fig. 15 closest to 228 MHz, (222,232) MHz have amplitudes of (2.92,3.62) kV/m. With the same current density as in the PIC-simulation the amplitudes become (10.2,12.7) kV/m which is in good agreement with the PIC field amplitude $\sim$ 11 kV/m.

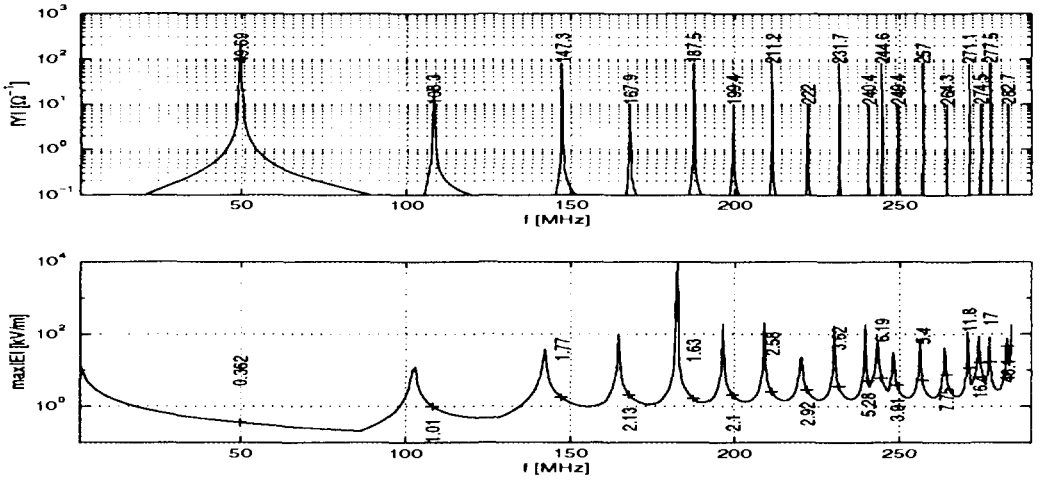

Figure 15: (a) The admittance $|Y| = 1/|Z|$ with diode area $A = 1$ m^2. The maximum admittance at the resonances are artificially limited. The amplitude is chosen for readability of the values that specifies the resonant frequencies in MHz. (b) The maximum magnitude of the electric field $\max_x |E_1(x)|$ as function of frequency. The printed values are the maximum field amplitude at the resonant frequencies in (a). The electron temperature is 10 eV, the current j_T =1 Am^{-2} and the static density profile and the static electric field is as shown in Fig. 9. Note that $\max |E_1|$ is unlimited at the discontinuities in $X(\omega)$, see Fig. 14.

The localization of the spikes for the resonant frequencies are shown in Fig. 13. As in the PIC simulation all maxima appear above of the resonant line $\omega = \omega_p(x)$. The lowest lying resonance has a spatially decaing solution with maximum at the cathode. The second resonance fits well to the lowest spike in the PIC-simulation (Fig. 3). The spike (232 MHz) coincide with the PIC spike both spatially and in frequency. There is not a perfect match $2f_1 = f_2$ but there are several approximations underlying the result in Figs. 13–15. The second resonance at 108 MHz is the lowest lying resonance that allows for beam modulation since there is no oscillating particle current at the cathode.

5 Eigenmodes of modified systems

In different PIC-simulations it has been hard to find the HF-spike. Minor changes of the temperature or ion profile have caused the disappearance of the spike. Some new examples that are slightly modified compared to the first example will be given. For each new example there will be an adaptive approach for the discretization in two steps, in analogy with the first example, but only the final results will be shown.

As was mentioned in the previous section the boundary condition $\alpha_{0,L} = 1$ in Eq. 5 is questionable. The oscillating particle current is not zero in the PIC-simulations. The solution for the other extreme assumption $\alpha_{0,L} = 0$, i.e., no displacement current at the boundary is shown in Figs. 16–18. The position of the maximum amplitude in Fig. 16 is qualitatively the same as with the boundary condition $\alpha_{0,L} = 1$ except for the lowest resonance. With no oscillating field at the boundary only growing solutions can be found. The previous resonance $f = 49.7$ MHz in Fig. 13 had a spatially decaying field

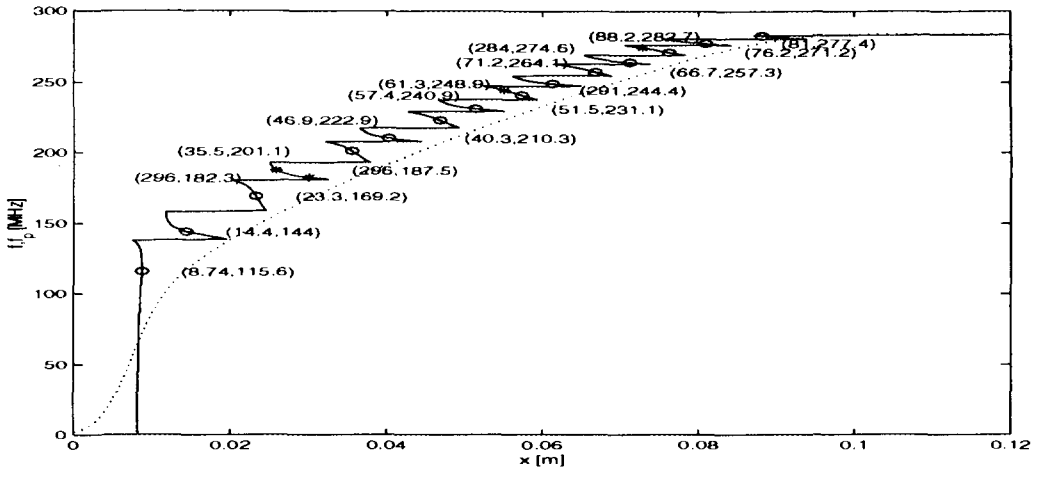

Figure 16: The sawtooth shaped line gives the position of the maximum field amplitude in the left part $x < 0.12$ m of the diode. For some frequencies this is not the global maximum. Resonant frequencies with maximum in the shown region are marked with circles and resonant frequencies with global maximum in the anode sheath are marked with stars. The position of the global maximum (x [mm],f [MHz]) are given in the parenthesis. The local plasma frequency is shown as reference by the dotted line. The electron temperature is 10 eV. The static density profile and the static electric field is as shown in Fig. 9. There is no displacement currents at the boundaries ($E_1|_{x=0,L} = 0$).

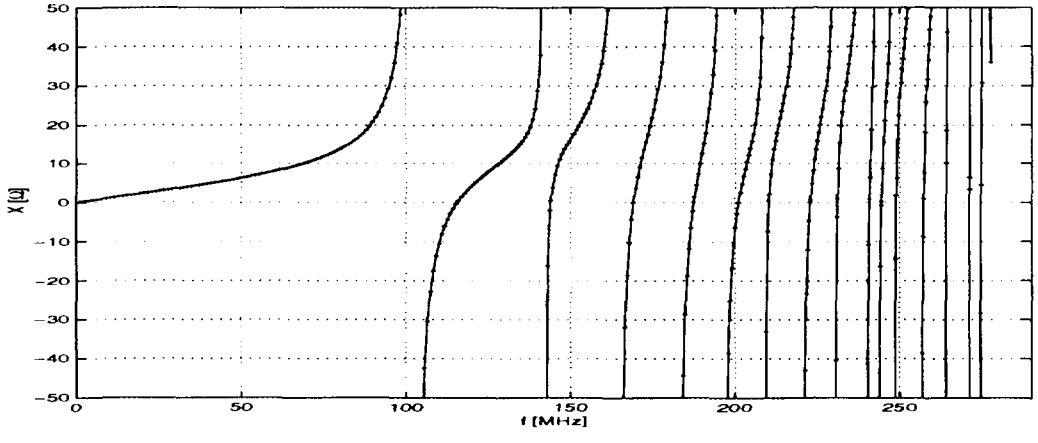

Figure 17: The reactance $X(\omega) = \Im Z(\omega)$ with diode area $A = 1$ m^2 and the electron temperature 10 eV. The static density profile and electric field is as shown in Fig. 9. The small dots are the calculated points. There is no displacement currents at the boundaries ($E_1|_{x=0,L} = 0$).

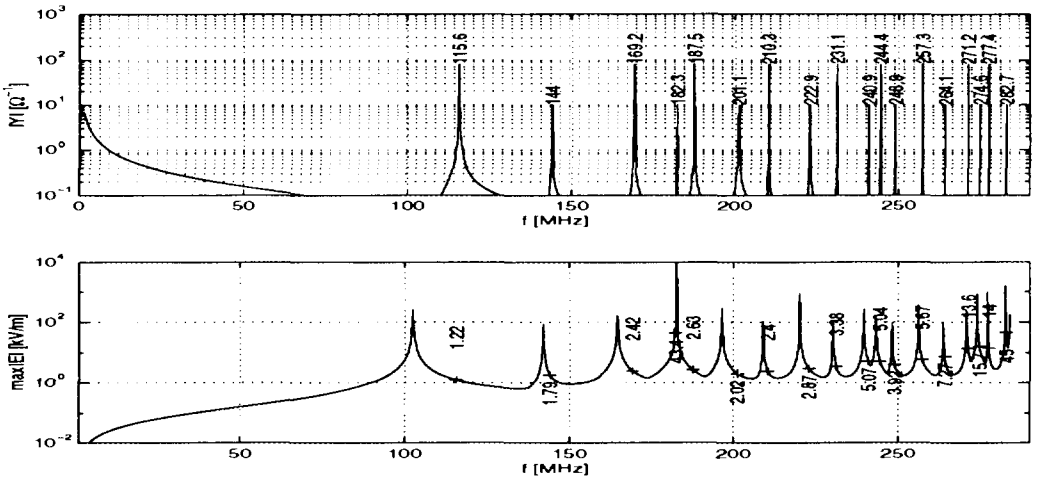

Figure 18: (a) The admittance $|Y| = 1/|Z|$ with diode area $A = 1$ m^2. The maximum admittance at the resonances are artificially limited. The oscillating amplitude is only chosen for readability of the values that specifies the resonant frequencies in MHz. (b) The maximum magnitude of the electric field as function of frequency. The printed values are the maximum field amplitude at the resonant frequencies in (a). The electron temperature is 10 eV, the current j_T =1 Am^{-2} and the static density profile and the static electric field is as displayed in Fig. 9. There is no displacement currents at the boundaries ($E_1|_{x=0,L} = 0$). Note that $\max|E_1|$ is unlimited at the discontinuities in $X(\omega)$, see Fig. 14.

amplitude. There is still an isolated low resonance around 110 Mhz and a more dense spectrum above it (Figs. 16, 18). The amplitudes at the new resonances have close to the same levels as with the other boundary conditions. The amplitudes and the pattern of the spectrum are thus robust to changes in the boundary condition. In Fig. 17 it is evident that there is a limiting resonance for low frequencies. With a boundary condition somewhere in between the two extremes, the lowest resonance will be found in the range 0-50 MHz. Low frequency modulations well below the spike frequency and clearly above typical ion frequencies have been found in a similar experiment [1]. These modulations could perhaps be an indication of an excited low resonance. If phase differences between the particle and total current are present at the boundaries ($\alpha \notin \Re$), the phase of E_1 will be spatially varying.

The average electron energy is different in different parts of the plasma column because of the acceleration of the beam component. The previous example (Figs. 8-18) was calculated for 10 eV electrons. In Fig. 10 the temperature in different parts of the diode is shown. In the wave cavity for the spike $x \in [0, 5.5]$ cm the temperature is clearly higher than 10 eV. With higher energy the thermal velocity and consequently the wavelength increases and the mode volume is expected to decrease. In Fig. 19 (with 20 eV) there is an reduced number of resonances. Except from the lowest resonance the resonant frequencies have increased and some resonances have been lost in the high frequency end. The wave part solution for the lowest frequency is in spatial regions of high static electric field. The higher temperature has decreased the static field and thereby reduced the growth rate and the wavelength (see the characteristic roots of Eq. 8). These effects from the

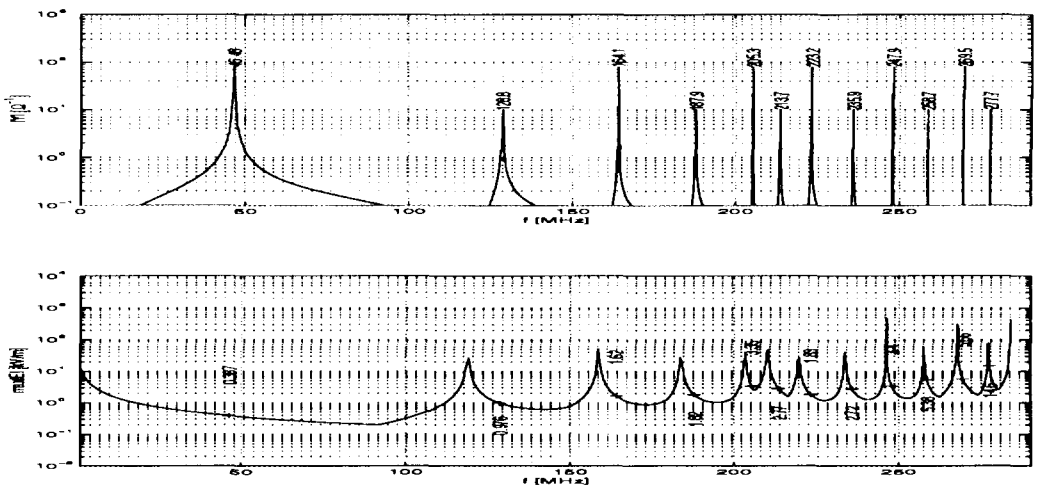

Figure 19: (a) The admittance $|Y| = 1/|Z|$ with diode area $A = 1$ m^2. The maximum admittance at the resonances are artificially limited. The oscillating amplitude is only chosen for readability of the values that specifies the resonant frequencies in MHz. b) The maximum magnitude of the electric field as function of frequency. The printed values are the field amplitude at the resonant frequencies in a). The electron temperature is 20 eV, the current j_T =1 Am^{-2} and the static ion density profile is as shown in Fig. 9.

increased E_0 seem to dominate over the increased wavelength caused by the reduced thermal velocity.

As reported in Sec. 2 the PIC simulations with mobile ions had to run for 2 μs before the spike appeared. During this time ions left the diode close to the anode. All presented figures of the eigenmodes are based on the ion profile in Fig. 9 with a depletion at the right boundary. The eigenmodes with homogeneous ion profile in the right end were calculated. Some of the anode (electron) cavity resonances then disappeared and the other resonant frequencies changed a few MHz. If the requirement of two resonances with $2f_1 = f_2$ is a necessary condition for spike formation and the resonances are sharp, the frequency shift could be a sufficient cause for the absence of the spike during the first 2 μs of the simulation.

The eigenmodes for a 1 m system with the same ion profile at the boundaries, i.e., with an extended homogeneous part were calculated. The electric field solutions in the wave part regions did not change and the homogeneous particular solution was the same. But a longer region with constant field gives larger contribution to the potential drop. To get resonances with $X = 0$ a more asymmetric, high amplitude field is required. Consequently the amplitudes at the resonances increase and the resonant frequencies are shifted closer the discontinuities in X. Close to the discontinuities the system is sensitive to f and narrow resonances are obtained.

6 Discussion

The behaviour of the fluid eigenmodes indicates that it is likely that the spike is a composition of excited eigenmodes. The maximum field amplitude at a position with local plasma frequency slightly below the spike frequency is ev-

ident in both the PIC-simulation and in the fluid description (Figs. 3,13,16). The spike amplitude evaluated theoretically is also in good agreement with the PIC-simulation. If the spike is a two frequency system of coupled oscillators, the narrowness of the resonances is a satisfactory explanation for the rarity of the spike and the sensitivity to different parameters. The growth rate in the PIC-simulation is higher than predicted by kinetic beam plasma theory, for infinite, homogeneous plasmas without static electric fields. The fluid eigenmode description, however, gives a correct estimate of the electric field amplitude at the spike.

Kinetic eigenmodes of the diodes would probably deviate from the idealized fluid picture. The beam acts as an energy pump exciting the eigenmodes. Not only Langmuir waves could propagate in the diode. The slow space charge wave is likely to be important in some regions. These waves could then explain the travelling waves observed in some regions [3]. Wave modes that have large deviation in the phase velocity compared with the Langmuir waves are damped. The pattern of the eigenmode spectrum is expected to be the same with new kinetic wave modes since they have the largest growth (or smallest damping) if they are closely resonant with the Langmuir waves in the fluid description.

Similar eigenmodes could probably exist in different systems in naturally occurring plasmas. The requirements for such systems to contain eigenmode structures are reflection points in a gradient, a closed current system with low losses and an energy pump to compensate for the losses. Systems containing reflection regions and electron beams are, e.g., ionisation double layers. High frequency electric field spikes have been measured at the high potential side of such double layers [1]. It is also possible that density cavities in space plasmas could contain eigenmodes of the kind described here. To determine the eigenmodes of such systems it is necessary to know the closed current systems. If the gradient part in any cavity contains many wavelengths the mode volume will be dense, regardless of the closure of the currents and the specific boundary conditions.

The low frequency f_1 and, by the high amplitude, the harmonic $2f_1$ can premodulate the beam. The f_1 resonance can gain energy from the beam plasma interaction in a limited region since the unstable bandwidth ends around $1.2f_p$. When entering the dense plasma also a kinetic model gives evanescent field solutions. It is questionable if this spatially limited growth is satisfactory to compensate for losses. The high resonance $f_2(= 2f_1)$ can gain energy in a region that is about a wavelength for the beam mode. By the reflected wave this wave energy is transported back to the first maximum. It is possible that this eigenmode f_2 feeds energy to f_1. The necessity of the frequency division is also an open question. The dominant loss mechanisms are particle acceleration in the spike and Landau damping of the backward wave. Both these processes accelerate particles that leaves the system after a transit time.

The eigenmodes are highly asymmetric coherent systems. They are likely to be a source of electromagnetic radiation.

The break down of the fluid picture close to the cathode introduce some modifications of the resonant frequencies. It is possible that non-linear and kinetic effects tune the resonances to match $2f_1 = f_2$. In the experiments

[1, 2, 3] the spike is frequent which indicate a softer coupling condition. The excited ion waves (Fig. 1) must modify the spectrum on the ion time scale. This could then give moving spikes in a broader region than the single electron time scale spike, as seen in experiments [1, 2, 3]. In absence of a non-linear kinetic self adjusting tuning, the spike would disappear during long periods when the matching condition is broken. It is also possible that the spike is a naturally stable configuration. In the simulations, the ion-profiles have been defined and locked. In the experiment, the ponderomotive force in the spike and ionizations by high energy electrons accelerated in the spike may influence the ion profile to fit into electron eigenmode situations.

Non-linear tuning introduces an alternative explanations for the field amplitude saturation. If the resonance spectrum is amplitude dependent only the amplitudes that gives a matching condition could survive. But in the presented results space charge limits seem to saturate the amplitude.

7 Acknowledgements

We wish to thank professor S. Torvén and Dr. M. Raadu for discussions about the fluid model and for proof reading the manuscript. This work was supported by the Swedish natural science research council.

References

[1] H. Gunell, N. Brenning, and S. Torvén, "Bursts of high-frequency plasma waves at an electric double layer," *Journal of Physics D: Applied Physics*, vol. 29, pp. 643–654, 1996.

[2] H. Gunell, J. P. Verboncoeur, N. Brenning, and S. Torvén, "Formation of electric field spikes in electron beam-plasma interaction," *Physical Review Letters*, vol. 77, pp. 5059–5062, 1996.

[3] H. Gunell and T. Löfgren, "Electric field spikes formed by electron beam-plasma interaction in plasma density gradients," *Physics of Plasmas*, vol. 4, pp. 2805–2812, 1997.

[4] H. Böhmer, E. A. Jackson, and M. Raether, "Quenching of the beam-plasma instability by mode mixing at a density discontinuity," *Physics of Fluids*, vol. 16, pp. 1064–1071, 1973.

[5] L. D. Bollinger, W. Carr, H. Liu, and M. Seidl, "Beam-plasma instability in an inhomogeneous plasma," *Physics of Fluids*, vol. 17, pp. 2142–2143, 1974.

[6] J. R. Pierce, "Limiting stable current in electron beams in the presence of ions," *Journal of Applied Physics*, vol. 15, pp. 721–726, 1944.

[7] M. Hörhager and S. Kuhn, "Weakly nonlinear steady-state oscillations in the Pierce diode," *Physics of Fluids B*, vol. 2, pp. 2741–2763, 1990.

[8] S. Kuhn, "Linear longitudinal oscillations in collisionless plasma diodes with thin sheaths. Part II. Application to an extended Pierce-type problem," *Physics of Fluids*, vol. 27, pp. 1834–1851, 1984.

[9] T. L. Crystal, P. C. Gray, W. S. Lawson, C. K. Birdsall, and S. Kuhn, "Trapped-electron effects on time-independent negative bias states of a collisionless single-emitter plasma device: Theory and simulation," *Physics of Fluids B*, vol. 3, pp. 244–254, 1990.

[10] S. Kuhn, "The physics of bounded plasma systems (BPS's): Simulation and interpretation," *Contributions to Plasma Physics*, vol. 34, pp. 495–538, 1994.

[11] T. Löfgren and H. Gunell, "Flexible simple-pole expansion of distribution functions," *Physics of Plasmas*, 1997. Accepted for publication. Preliminary scheduled for the October 1997 issue.

[12] J. P. Verboncoeur, M. V. Alves, V. Vahedi, and C. K. Birdsall, "Simultaneous potential and circuit solution for 1D bounded plasma particle simulation codes," *Journal of Computational Physics*, vol. 104, pp. 321–328, 1993.